HO + CO Reaction Rates and H/D Kinetic Isotope Effects: Master Equation Models with ab initio SCTST Rate Constants.

ARTICLE *in* THE JOURNAL OF PHYSICAL CHEMISTRY A · JANUARY 2013

Impact Factor: 2.69 · DOI: 10.1021/jp311928w · Source: PubMed

4 AUTHORS:

Ralph E. Weston
Brookhaven National Laboratory
100 PUBLICATIONS **1,684** CITATIONS
SEE PROFILE

Thanh Lam Nguyen
University of Texas at Austin
72 PUBLICATIONS **1,373** CITATIONS
SEE PROFILE

John F Stanton
University of Texas at Austin
5 PUBLICATIONS **73** CITATIONS
SEE PROFILE

John R. Barker
University of Michigan
170 PUBLICATIONS **5,890** CITATIONS
SEE PROFILE

THE JOURNAL OF PHYSICAL CHEMISTRY A

Article

pubs.acs.org/JPCA

HO + CO Reaction Rates and H/D Kinetic Isotope Effects: Master Equation Models with ab Initio SCTST Rate Constants

Ralph E. Weston, Jr.,[†] Thanh Lam Nguyen,[‡] John F. Stanton,*[,‡] and John R. Barker*[,§]

[†]Department of Chemistry, Brookhaven National Laboratory, Upton, New York 11973, United States

[‡]Department of Chemistry and Biochemistry, The University of Texas, Austin, Texas 78712-0165, United States

[§]Department of Atmospheric, Oceanic, and Space Sciences, University of Michigan, Ann Arbor, Michigan 48109-2143, United States

Supporting Information

ABSTRACT: Ab initio microcanonical rate constants were computed using Semi-Classical Transition State Theory (SCTST) and used in two master equation formulations (1D, depending on active energy with centrifugal corrections, and 2D, depending on total energy and angular momentum) to compute temperature-dependent rate constants for the title reactions using a potential energy surface obtained by sophisticated ab initio calculations. The 2D master equation was used at the $P = 0$ and $P = \infty$ limits, while the 1D master equation with centrifugal corrections and an empirical energy transfer parameter could be used over the entire pressure range. Rate constants were computed for 75 K $\leq T \leq$ 2500 K and $0 \leq [\mathrm{He}] \leq 10^{23}$ cm^{-3}. For all temperatures and pressures important for combustion and for the terrestrial atmosphere, the agreement with the experimental rate constants is very good, but at very high pressures and $T \leq 200$ K, the theoretical rate constants are significantly smaller than the experimental values. This effect is possibly due to the presence in the experiments of dimers and prereactive complexes, which were not included in the model calculations. The computed H/D kinetic isotope effects are in acceptable agreement with experimental data, which show considerable scatter. Overall, the agreement between experimental and theoretical H/D kinetic isotope effects is much better than in previous work, and an assumption of non-RRKM behavior does not appear to be needed to reproduce experimental observations.

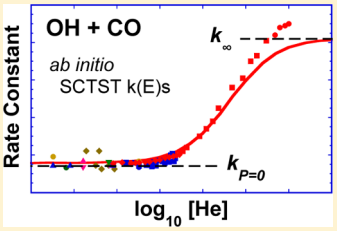

INTRODUCTION

The oxidation of carbon monoxide to carbon dioxide by the hydroxyl radical is important at high temperatures in combustion chemistry[1] and in the terrestrial atmosphere, where it is a major sink for the hydroxyl radical (the reaction HO + CH_4 is of comparable importance).[2] On the surface of Venus, where the atmosphere contains >90 bar of CO_2 and the temperature is ∼730 K due to the natural greenhouse effect, the reaction plays a key role in the cycling of carbon dioxide.[3] Because the reaction is a key step in so many important chemical systems, it has been the subject of a vast number of experiments, in which rate constants for the forward reaction have been obtained over a wide range of temperatures and pressures.[4−56] It soon became apparent that the reaction rate was dependent on total pressure and that the temperature dependence was non-Arrhenius. Smith and Zellner[11,51] were apparently the first to suggest that the reaction involved formation of an HOCO species (originally considered a collision complex) that could be stabilized by collisions and either dissociate back to reactants or form products.

Experiments have also determined the effect on the rate constant of isotopic substitution of DO for HO[20,24,28,36,57] and of ^{17}O, ^{18}O, and ^{13}C in carbon monoxide.[23,52−55] The dynamics of the reaction have been investigated by various methods. Early attempts[14] to find vibrational excitation in the carbon dioxide product were unsuccessful. Later, tunable diode laser spectroscopy enabled Smith and co-workers[30−32] to determine that not more than 6% of the available energy was found in the CO_2 product. They were also able to compare reaction rates of HO and DO in states $v = 0$ and $v = 1$.[28,57] Molecular beam experiments have also provided information about the dynamics of the reaction.[56] In photodetachment experiments on the $HOCO^-$ anion, the HO + CO, HOCO, and H + CO_2 products are observed.[58−61]

The reaction system has become a benchmark for kinetics and dynamics calculations because it is small enough for accurate quantum mechanical methods to be applied. Moreover, all of the reactions in the system have intrinsic energy barriers (i.e., there are no problems associated with barrierless reactions), quantum mechanical tunneling is important, the system consists of multiple wells and multiple reaction channels (but is not too complex), and prereactive complexes are present. In short, it is a prototype for complicated chemical activation reactions.

The important features of the potential energy surface (PES) for this reaction are shown in Figure 1. Energies of important points on this surface have been calculated with ab initio methods of various levels of sophistication by many research groups.[62−72] Statistical or RRKM calculations of rate constants have been based on the results of these ab initio calculations and on more or less ad hoc values for the parameters needed in the calculations.[35,73−78] Rate constants have also been obtained

Received: December 4, 2012
Revised: January 14, 2013
Published: January 14, 2013

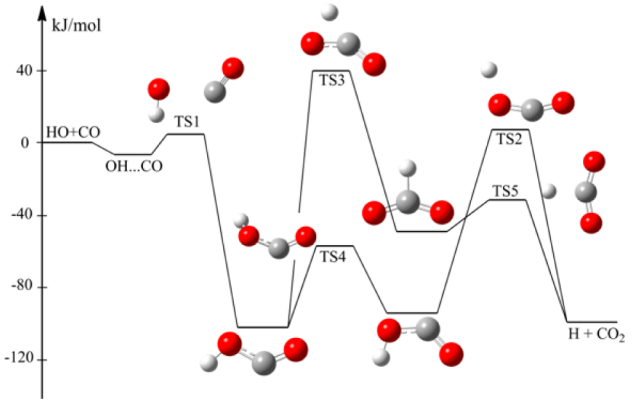

Figure 1. Potential energy surface of the HOCO reaction system. Reprinted from ref 72. Copyright 2012 American Chemical Society.

using methods of quantum reactive scattering.[79−83] Finally, quasiclassical trajectory calculations have been carried out, usually on analytical surfaces derived from ab initio calculations.[81,84−88]

The global reaction expresses the loss of HO radicals:

$$HO + CO \rightarrow \text{products} \quad \text{(R1)}$$

The complete reaction scheme below reflects the importance of the *cis*- and *trans*-HOCO intermediates, which react differently:

$$HO + CO \rightleftarrows \textit{trans}\text{-HOCO}^* \quad \text{(R1a, −R1a)}$$

$$\textit{trans}\text{-HOCO}^* \rightarrow H + CO_2 \quad \text{(R2)}$$

$$\textit{trans}\text{-HOCO}^* \rightleftarrows \textit{cis}\text{-HOCO}^* \quad \text{(R4, −R4)}$$

$$\textit{cis}\text{-HOCO}^* \rightarrow H + CO_2 \quad \text{(R3)}$$

$$\textit{trans}\text{-HOCO}^* + M \rightleftarrows \textit{trans}\text{-HOCO} + M \quad \text{(R5, −R5)}$$

$$\textit{cis}\text{-HOCO}^* + M \rightleftarrows \textit{cis}\text{-HOCO} + M \quad \text{(R6, −R6)}$$

where the asterisk denotes significant rovibrational excitation and M is a chemically inert bath gas.

Previously, we applied ab initio Semi-Classical Transition State Theory (SCTST) to reaction R1 in order to predict the limiting zero- and high-pressure rate constants and to evaluate the contribution of quantum mechanical tunneling to the thermal rate constants.[72] In the present article, we extend that work to the intermediate pressure range and to the calculation of kinetic isotope effects (KIEs). SCTST, which was developed by W. H. Miller and colleagues,[89−92] is a powerful theory that intrinsically includes zero-point energy, multidimensional quantum tunneling along the curved reaction path, anharmonicity, and nonseparable coupling among all vibrational degrees of freedom, including the reaction coordinate. In recent tests made using our new implementation of SCTST,[93,94] the CFOUR electronic structure code[95] was used to calculate highly accurate thermochemistry. The vibrational anharmonicities (X_{ij}) of reactants, products, and transition states were computed using a modified version of CFOUR that employs analytical first and second derivatives for coupled cluster theory with single and double excitations and a perturbative treatment of triple excitations (CCSD(T)).

In addition to the computation of canonical rate constants, SCTST provides the microcanonical rate constants that are required for master equation calculations. Except for a demonstration calculation,[93] the present work is the first serious application of SCTST to pressure-dependent master equation simulations.

Part of the motivation of the present work was to extend our previous study of reaction R1 to lower temperatures. In ref 72, we reported thermal rate constants at the zero pressure and infinite pressure limits, based on ab initio SCTST microcanonical rate constants. At $P = 0$, the explicit 2-dimensional master equation, which depends on both total energy and angular momentum (i.e., the 2D master equation depends on E and J), can be solved exactly,[96−101] as pointed out in ref 72. The rate constants at $P = 0$ and $P = \infty$ were found to be in excellent agreement with the experimental data over the range from 250 to 2500 K. In the present work, we extend the temperature range to below 100 K. We also use a conventional 1D master equation (depending only on E) with centrifugal corrections and empirical energy transfer parameters to model the intermediate pressure range.

As described in the present work, the results of the 1D master equation simulations differ somewhat from the exact solutions of the 2D master equation. Both master equation simulations differ from the experiments under conditions of simultaneous extreme low temperature and high-pressure, possibly due to the presence of prereactive complexes and dimers, which are not included in the calculations. Nonetheless, the 1D master equation simulations, which utilize ab initio SCTST rate constants and empirical energy transfer parameters, provide a very good description of the experimental data over the entire range of temperatures and pressures found in the terrestrial atmosphere and in combustion. In the Appendix, we discuss the technical differences between the 1D and 2D master equation treatments.

A second motivation for the present work was to determine whether the ab initio SCTST rate constants can predict the H/D kinetic isotope effects (KIEs) accurately for reaction R1. In an application of SCTST to the study of KIEs in the Cl + CH_4 reaction, it was found that the predicted H/D KIEs are as accurate as the experimental data, but the $^{12}C/^{13}C$ KIEs are not.[102] In previous work, the H/D KIEs for reaction R1 have resisted theoretical interpretation. Chen and Marcus reported that standard RRKM theory (with Eckart tunneling corrections) could not account successfully for the H/D KIEs for reaction R1 and that a novel non-RRKM model was required.[70,103,104] In contrast, it is found in the present work that the H/D KIEs calculated by using the ab initio SCTST rate constants are in reasonable agreement with the experimental data, perhaps showing that the difficulties encountered in earlier studies were due to inadequate treatments of tunneling.

In the next section, the theoretical methods are described. Following that section, we describe the results of our calculations of the pressure and temperature dependence of reaction R1. The computed H/D KIEs are then described, followed by our conclusions. All of the parameters used in the kinetics calculations can be found in ref 72 or in the present work.

THEORETICAL METHODS

Ab Initio Calculations. As reported in ref 72, the energies of all stationary points including minima and transition structures on the lowest-lying doublet electronic PES were computed using the HEAT protocol (see Figure 1).[105−107] This model chemistry includes a treatment of electron correlation that includes quadruple excitations (the variant used here is HEAT-345Q[108]) and does not contain any empiricism apart

Table 1. Calculated Classical Energies[a] (kcal mol^{-1}) of Stationary Points on the HOCO PES

method	G2M/MP2	FCC/CBS F12	MRCISD+Q/cc−pVTZ	CCSD(T)	HEAT
ref	69	67	71	85	72
HO + CO	0.0	0.000	0.00	0.00	0.00
HO···CO	−2.3	−2.196	−1.66	−2.26	−2.59
HO···OC	−1.4	−1.128	−0.17	−1.22	−0.84
trans-HOCO	−28.5	−30.103	−27.69	−29.59	−29.43[b]
cis-HOCO	−26.7	−28.248	−25.84	−27.82	−27.71
trans-TS1	−1.0	−0.959	−2.73	−0.58	−0.63
cis-TS2	2.3	1.439	2.93	2.41	2.50
torsion-TS	−10.1	−20.776	−18.35	−20.29	−20.14
HCO2	−11.7	−14.580	−13.48	−13.84	−12.85
trans-TS3	9.6	7.856	10.52	8.78	8.92
C2v-TS5	−8.8	−9.839	−9.62	−8.71	−8.19
H + CO2	−23.5	−23.393	−23.14	−23.02	−23.54

[a]Vibrational zero-point energies are not included. [b]The atomization energy agrees with the value obtained by Feller et al.[110] within ∼0.6 kcal mol^{-1}.

from that associated with basis set extrapolation techniques and the use of experimental spin−orbit corrections. In addition to the vibrational zero-point energy, other small adjustments such as scalar relativistic correction, first-order spin−orbit coupling, and the diagonal Born−Oppenheimer correction are included. For an elaborated discussion of the HEAT protocol and the accuracy that has been obtained by this procedure for thermochemical parameters, the interested reader is referred to refs 105−107.

For minima on the potential energy surface, HEAT has a demonstrated ability to predict bond energies to within 1 kJ mol^{-1}; for transition states where the single-reference approach is still adequate (as in the case here), a similar accuracy might be expected. The computed classical energies (i.e., omitting zero-point energy corrections) are tabulated in Table 1. Unlike the original papers, in this work, we use zero-point anharmonic vibration energies (ZPE) obtained with CCSD(T) (in the frozen core approximation) in combination with the atomic natural orbital (ANO) basis set of Almlof and Taylor.[108] A truncated ANO basis set, here referred to as ANO1, with the truncation of 4s2p1d for the H atom and 4s3p2d1f for the non-hydrogen atoms, was used to obtain the anharmonic force. The harmonic force fields were computed with the ANO2 basis set, which is contracted as 4s3p2d1f for H atom and 5s4p3d2f1g for C and O atoms. Second-order vibrational perturbation theory (VPT2)[109] was then used to compute the fundamental vibrational frequencies, which are reported elsewhere.[72] The zero-point energy, including the constant term that is not relevant to optical spectroscopy, was computed with VPT2.[94] The CFOUR program package[95] was used for all electronic structure calculations.

The thermochemical results obtained using HEAT can be found in ref 72 (HOCO) and in the Supporting Information for the present work (HOCO and DOCO). The thermochemical values are in reasonable agreement with previous theoretical work, considering the methods used and their uncertainties. By using the total atomic energy calculated in the present work for *trans*-HOCO (382.9 ± 0.3 kcal mol^{-1}) and the experimental enthalpies of formation for H, C, and O, we obtain the enthalpy of formation of *trans*-HOCO at 0 K, ΔH_f(*trans*-HOCO) = −43.3 ± 0.3 kcal mol^{-1}. This value is in reasonable agreement with the −43.9 ± 0.5 kcal mol^{-1} obtained by Feller et al.,[110] who used CCSD(T) extrapolated to the complete basis set limit, various other small corrections, and zero-point energies obtained by weighted averages of experimental fundamental frequencies and theoretical harmonic frequencies. We also find that *cis*-HOCO is less stable than *trans*-HOCO by 1.5 kcal mol^{-1}, which is in good agreement with the other recent theoretical values listed in Table 1 of ref 72. In contrast, Feller et al. reported in the text of their paper that *cis*-HOCO is 2.9 kcal mol^{-1} less stable than the trans isomer at 0 K. This energy difference is ≥1 kcal mol^{-1} larger than any of the other theoretical values. If this is not a typographical error, a detailed analysis would be needed to identify all of the differences between the theoretical methods used by Feller et al. and those used in the present work, but it is possible that the ad hoc method used by Feller et al. for determining the zero-point energies is a contributing factor.

Chemical Kinetics Calculations. For reactions that include bound intermediates, a master equation formulation must be used in order to account for energy, angular momentum, and the effects of collisions. In the limits of zero-pressure (i.e., in the complete absence of collisions) and infinite pressure (i.e., for strictly canonical energy distributions), the master equation simplifies and can be solved analytically. At intermediate pressures (i.e., in the pressure falloff regime), one must use numerical master equation techniques.

As previously reported in ref 72, analytical solutions of the two-dimensional master equation (i.e., depending on both energy and angular momentum) exist at the zero and infinite pressure limits, enabling calculation of the rate constant[35,98,111] for the reaction HO + CO → H + CO_2:

$$k_{P=0}(T) = \frac{1}{h}\frac{Q^{\neq}_{\mathrm{trans,elec}}}{Q_{\mathrm{HO}}Q_{\mathrm{CO}}}\sum_{J=0}^{+\infty}(2J+1)\int_0^{+\infty}\frac{G_1^{\neq}(E,J)G_{23}^{\neq}(E,J)}{G_1^{\neq}(E,J)+G_{23}^{\neq}(E,J)}\exp\left(-\frac{E}{k_BT}\right)\mathrm{d}E \quad (1a)$$

$$G_{23}^{\neq}(E,J) = G_2^{\neq}(E,J) + G_3^{\neq}(E,J) \quad (1b)$$

$$k_{P=\infty}(T) = \frac{1}{h}\frac{Q^{\neq}_{\mathrm{trans,elec}}}{Q_{\mathrm{HO}}Q_{\mathrm{CO}}}\sum_{J=0}^{+\infty}(2J+1)\int_0^{+\infty}G_1^{\neq}(E,J)\exp\left(-\frac{E}{k_BT}\right)\mathrm{d}E \quad (2a)$$

dx.doi.org/10.1021/jp311928w | J. Phys. Chem. A 2013, 117, 821−835

Table 2. Collision Parameters[a] for HO + CO and DO + CO[b]

species	σ (Å)	ε (K)	α (cm^{-1})	comments	ref
HOCO	4.00	X (190?)		based on CO_2 from ref 146, who cited ref 147	76
	4.00	200		following refs 130. 148,	35
	X	X		parameters from ref 35?	36
	4.55	260		from MP2 calculations	69
	4.00	200			78
	4.00	300		(see text)	this work
He	2.55	10	150		35
	X	X	$\langle\Delta E\rangle_{all}$ = 53	others from ref 35?	36
	2.55	10	150	σ and ε from ref 149	69
	3.94	201	150	σ and ε for HOCO + M pair, from ref 149; α = 180 cm^{-1} at 250 K; α = 180 cm^{-1} for DOCO	73
	2.58	10.2	150		78
	X	X	80 × $(T/300)^{0.85}$	α for HOCO + M pair	74
	2.55	10	140	σ and ε from ref 69, who cited ref 149; stepladder model; nonstatistical α = 140 cm^{-1}	70
	2.55	10	125	σ and ε from ref 149; $\alpha \approx$ 200 cm^{-1} at high P (see text)	this work
Ar	X	X	$\langle\Delta E\rangle_{all}$ = X	others from ref 35?	36
	3.47	114	400	σ and ε from ref 149	69
	X	X		α = 300 cm^{-1} for DOCO	73
	3.47	114		σ and ε from ref 69, who cited ref 149; stepladder model; α = 190 cm^{-1} for DOCO; nonstatistical α = 190 cm^{-1} for DOCO	70
	3.33	136.5	260		78
N_2	X	X	$\langle\Delta E\rangle_{all}$ = 210	others from ref 35?	36
	3.74	82	250	σ and ε from ref 149	69
	X	X	300	α = 480 cm^{-1} for DOCO	73
	3.62	97.5	250		78
			100 × $(T/300)^{0.85}$	α for HOCO + M pair; α = 140 cm^{-1} for DOCO	74
	3.74	82	200	σ and ε from ref 69, who cited ref 149; stepladder model; nonstatistical α = 210 cm^{-1}	70
	4.00	200	160	for HOCO + M pair	75
	3.74	82	250	σ and ε from ref 149	this work
CF_4	4.40	166	450	σ and ε from ref 149	69
	X	X	680	α = 680 cm^{-1} for DOCO	73
	4.40	166	675		78
	X	X	160 × $(T/300)^{0.85}$	α for HOCO + M pair; α = 150 cm^{-1} for DOCO	74
	4.40	166	300	σ and ε from ref 69, who cited ref 149; stepladder model; nonstatistical α = 310 cm^{-1}	70
	4.40	166	~700	σ and ε from ref 149	this work
SF_6	2.50	X (259?)		from ref 146	76
	5.20	212	1000	σ and ε from ref 149	69
	X	X	800	α = 800 cm^{-1} for DOCO	73
	5.50	276	1200		78
	X	X	160 × $(T/300)^{0.85}$	α for HOCO + M pair; α = 200 cm^{-1} for DOCO	74
	5.20	212	410	σ and ε from ref 69, who cited ref 149; stepladder model; nonstatistical α = 400 cm^{-1}	70
	5.20	212	~2000	σ and ε from ref 149	this work

[a] σ and ε (Lennard-Jones parameters) and $\alpha \approx -\langle\Delta E\rangle_{down}$ (the average energy transferred in deactivating collisions) for conventional exponential-down model at ~300 K, unless otherwise noted. X denotes parameter values that were not specified in the original papers. Question marks indicate ambiguity in the original paper. [b] Parameters listed in comments column.

$$k_{P=\infty}(T) = \frac{k_B T}{h}\frac{Q^{\neq}_{TS1}}{Q_{HO}Q_{CO}}\exp\left(-\frac{\Delta E^{\neq}_{TS1}}{k_B T}\right) \quad (2b)$$

In these equations, h is Planck's constant, k_B is Boltzmann's constant, and Q_{HO}, Q_{CO}, and $Q^{\neq}_{TS1}$ are total partition functions of HO, CO, and TS1, respectively. The electronic partition function of HO is given by $Q^{elec}_{HO} = 2 + 2\exp(-139\text{cm}^{-1}/k_B T)$. The factor $Q^{\neq}_{trans,elec}$ is the product of translational and electronic partition functions corresponding to transition structure TS1. Factors $G^{\neq}_1(E,J)$, $G^{\neq}_2(E,J)$, and $G^{\neq}_3(E,J)$ are the rovibrational cumulative reaction probabilities (CRP) at each (E,J) for TS1, TS2, and TS3, respectively. As explained in ref 72, the isomerization reaction (TS4) can be neglected at steady-state when P = 0. In these expressions, the $2J$ + 1 rotational degeneracy factor is written explicitly. Vibration and rotation are assumed to be separable, so $G(E,J)$ can be computed by convolution and is expressed as

$$G(E,J) = \int_0^E G_{vib}(E - E_{rot})\rho_{rot}(E_{rot})\mathrm{d}E_{rot} \quad (3)$$

Here, the vibrational CRP, $G_{vib}(E)$, is calculated using SCTST,[93,94] which naturally includes fully coupled vibrations and multidimensional tunneling. As explained in ref 72, rotational energy levels of a rigid symmetric top molecule are used for three of the transition states, with the constraint $-J \le K \le J$. In ref 72, both the CRP and the rotational density of states are obtained by explicit state counting, using an energy bin of 1 cm^{-1}, a maximum J of 200, and a ceiling energy of 5 × 10^4 cm^{-1} relative to the initial reactants. The latter two quantities are chosen to be sufficiently high to ensure that all

reaction rate constants in the temperature range from 50 to 2500 K have converged numerically. The summation and integral in eqs 1a and 2a are computed by a simple summation using step sizes of 10 cm^{-1} and unity for E and J, respectively, and the relative errors are less than ±0.2%.[72]

Rate constants in the intermediate pressure regime (i.e., in the falloff) are computed using the MultiWell Software Suite of programs.[112−114] The MultiWell master equation code depends explicitly on active energy; angular momentum conservation is included approximately via centrifugal corrections.[115] Although it would be more desirable to use an explicit 2D master equation (depending explicitly on both energy and angular momentum) for the falloff regime, the task of developing such a code is beyond the scope of the present work. However, the 1D MultiWell master equation code (depending explicitly on active energy) is in exact agreement with eq 2 at $P = \infty$ limit and is in good, but not exact, agreement with the solution at the $P = 0$ limit, as discussed below.

For the 1D master equation simulations, the multiwell, multichannel model consisted of *cis*- and *trans*-HOCO and reactions via TS1, TS2, TS3, and TS4; HCO_2 and the weakly bound prereactive complexes were neglected. At low energies (i.e., during and after vibrational deactivation), it cannot be assumed that *cis*- and *trans*-HOCO are in equilibrium (unlike in ref 72), and thus, the isomerization reaction (TS4) was considered explicitly and treated as reversible. Microcanonical rate constants, $k(E)$, were computed for all of these reactions:

$$k_i(E) = \frac{L_i^{\ddagger}}{h}\frac{G_i^{\ddagger}(E - E_{0r,i})}{\rho_{R,i}(E)} \tag{4}$$

where for the ith reaction, $L_i^{\ddagger}$ is the reaction path degeneracy, h is Planck's constant, $G_i^{\ddagger}(E - E_{0r,i})$ is the CRP, E is the active energy of the reactant, $E_{0r,i}$ is the critical energy (with centrifugal correction; see Appendix), and $\rho_{R,i}(E)$ is the density of states for the reactant. The densities of states for the fully-coupled anharmonic vibrations were computed using computer code ADENSUM (part of the MultiWell Software Suite), which uses an algorithm[116] that is based on the work of Basire et al.[117] and Wang and Landau.[118] The CRPs were computed using computer code SCTST (part of the MultiWell Software Suite), which implements SCTST, as documented elsewhere.[93,94] The critical energies computed using the HEAT protocol were used without adjustment.

When computing the CRPs and densities of states, one external rotational degree of freedom (the K-rotor) was assumed to be completely active (i.e., its energy can randomize, along with the energy in the vibrational modes) and completely independent of the total angular momentum. When centrifugal corrections are used, this separable rotors approximation[119] is commonly employed in place of the exact constraint that the K quantum number is limited by the quantum number J for total angular momentum: $-J \le K \le +J$.[120−122] In the present work, all chemical species were approximated as symmetric tops with $A \neq B = C$ (rotational constants A, B, and C). Current and Rabinovitch showed that the separable rotors approximation is most accurate when the rotational constants for the K-rotor and the and 2D adiabatic rotor are given by $B_K = A$ and $B_{2D} = (BC)^{1/2}$, respectively.

Collisional energy transfer involving *cis*- and *trans*-HOCO was treated as the product of the Lennard-Jones (L-J) collision frequency multiplied by the probability density function for the conventional exponential-down step size distribution:[112,113]

$$P(E, E') = N^{-1}\exp[(E - E')/\alpha] \quad \text{for } E \le E' \tag{5}$$

where E and E' are the final and initial energies, respectively, N is a normalization factor, and α is an adjustable parameter that is approximately equal to the magnitude of $\langle\Delta E\rangle_{down}$, the average amount of energy transferred in deactivating collisions. The same value of α was used for both HOCO isomers.

The L-J parameters used in the present work for the HOCO intermediates and bath gases are presented in Table 2. The L−J parameters used for the bath gases are standard values found in the literature (see Table 2 for literature citations). The parameters for the HOCO intermediates adopted by most previous workers were based on the L-J parameters for CO_2 (see Table 2). In the present work, we adopted the value for $\sigma(CO_2)$, but we arbitrarily assumed that the L-J well-depth for HOCO is about 100 K deeper than $\varepsilon(CO_2)$ due to the polar attraction of the HO group that is present in HOCO, but not in CO_2. Zhu et al. concluded on the basis of electronic structure calculations (MP2 level of theory) that both L-J parameters for HOCO are larger than those for CO_2,[69] a conclusion that is qualitatively consistent with our assumption. The effect of ε is not large, except at very low temperatures, and errors in the assumed L-J parameters can be compensated by empirical adjustments of parameter α.

The MultiWell stochastic simulations were initiated by assuming that *trans*-HOCO is formed by reaction R1 with a nascent chemical activation energy distribution.[112,123] An energy grain of 5 cm^{-1} was used computing the CRPs and densities of states; the energy ceiling for the master equation calculations was 49 500 cm^{-1}. The energy grain of 5 cm^{-1} employed in the present 1D master equation calculations produces results at the high pressure limit that are essentially indistinguishable from those obtained in ref 72 with the energy grain of 1 cm^{-1}. Gillespie's stochastic simulation algorithm[124,125] was used to produce the simulations. No special constraints or assumptions were imposed on the simulations, which produced records of the time-dependent relative concentrations of the intermediates (i.e., *cis*- and *trans*-HOCO) and products (i.e., HO + CO and H + CO_2). Rate constants were obtained from the time-dependent results by an analysis that is described in the Results and Discussion section. The simulations were carried out in batches of 10^5 to 10^6 stochastic trials at each temperature (from 75 to 2500 K) and collider gas number density [M] = 10^{10} to 10^{23} molecules cm^{-3}.

RESULTS AND DISCUSSION

Overview. The first step of the global reaction is the formation of nascent excited *trans*-HOCO via transition state TS1. (We neglect the prereactive complex.[72]) The rate of formation of nascent *trans*-HOCO is proportional to the corresponding high-pressure limit rate constant $k_{1a,\infty}$. The nascent chemical activation energy distribution is related to the thermal energy distribution of HO and CO by detailed balance.[122] At 1000 K, for example, the nascent chemically activated *trans*-HOCO excitation energy (in addition to its zero-point energy) averages at about 11 220 cm^{-1}. Because the imaginary frequency in TS1 is small, tunneling is relatively unimportant, but because of tunneling, some of the excited *trans*-HOCO is formed at energies lower than the reaction critical energy defined in the absence of tunneling (the no-tunneling threshold). The microcanonical rate constants and no-tunneling thresholds are shown in Figure 2.

dx.doi.org/10.1021/jp311928w | J. Phys. Chem. A 2013, 117, 821−835

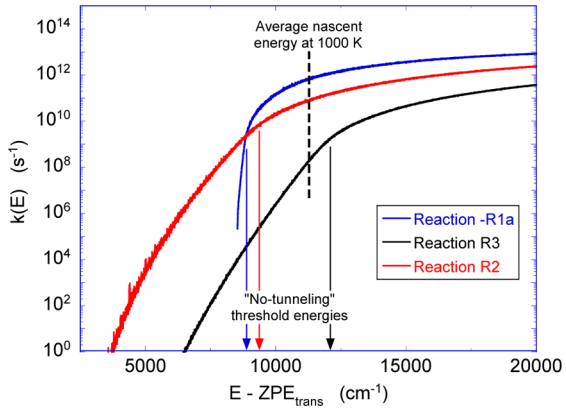

Figure 2. Microcanonical rate constants and no-tunneling reaction thresholds. Also shown is the average excitation energy of nascent *trans*-HOCO at 1000 K.

To avoid clutter in Figure 2, the microcanonical rate constants for the forward and reverse isomerization reactions are not shown, but they are $>10^{11}$ s^{-1} at energies $\geq$ 3000 cm^{-1} and $\gtrsim 3 \times 10^{12}$ s^{-1} at the energy of TS1. With such large isomerization rate constants, *cis*- and *trans*-HOCO rapidly come into microcanonical equilibrium with each other, justifying the assumption in deriving eq 1. *trans*-HOCO can react via TS3 and *cis*-HOCO can react via TS2 to produce H + CO_2. *trans*-HOCO can also react via TS1 to regenerate HO + CO. Even at temperatures below 100 K, the average energy of nascent *trans*-HOCO is greater than the no-tunneling threshold energy, and the rate of dissociation to HO + CO is significantly greater than that for producing H + CO_2. In the absence of collisions, the yield of H + CO_2 is governed by the nascent chemical activation energy distribution, which determines the competition between regeneration of HO + CO and production of H + CO_2, as embodied in eq 1.

When the bath pressure is high enough, the excited HOCO isomers can engage in collisional energy transfer before they react. As a result, the energy distributions broaden, and the mean energies decrease as the transient energy distributions tend to relax collisionally toward a steady-state (the falloff distribution). This process tends to reduce the average energies of the reacting isomers and hence reduce the reaction rates. Because tunneling is very important for reactions via TS2 and TS3, which have relatively large imaginary frequencies, the $k(E)$s for those reactions decrease more slowly as the average energy decreases than that of the $k(E)$ for reaction via TS1, which has a low imaginary frequency. Furthermore, at very high pressures and low temperatures, the HOCO isomers are essentially thermalized at such low energies that even the rate of tunneling is very low. In other words, as the energy decreases, the back-reaction to regenerate HO + CO slows down more than the forward reactions that produces H + CO_2, and the global reaction rate increases with pressure.

At low temperatures and high pressures, the HOCO isomers react very slowly. The thermalized HOCO isomers react primarily via TS2 and to a lesser extent via TS3, which has a much higher energy barrier, as shown in Figure 2; relatively little reacts via TS1 at low temperatures. In real chemical systems, the thermalized HOCO isomers may live long enough to undergo bimolecular reactions with other species (e.g., O_2).[126] At high temperature and high pressure, the HOCO isomers in their steady-state energy distributions have short lifetimes, which may compete with the rate of collisional energy transfer. Under the conditions considered in the present work, however, the time scales for collisional energy relaxation and chemical reaction are reasonably well separated, as discussed in the next section.

Rate Constants. *Determination of Rate Constants.* The master equation simulations produce time-dependent concentration profiles, from which reaction rate constants can be extracted, much as in experiments. In the experiments reported in the literature, the reaction rate constant for reaction R1a was determined by monitoring the decay of HO free radicals under various conditions of temperature and pressure, as illustrated in Figure 3. The initial step produces *trans*-HOCO in a nascent chemical activation population distribution. At the high-pressure limit, every nascent HOCO molecule is collisionally stabilized, and thus, the maximum measured rate constant must correspond to $k_{1,\infty}$. At lower pressures, some of the nascent HOCO can react by regenerating HO + CO, which reduces the net reaction yield; the rate constant is reduced in proportion (see eq 6).

When modeling the chemical activation process, the master equation simulations predict the fraction, f_{HO+CO}, of HO + CO that is regenerated as a function of time, or number of collisions, following formation of the nascent *trans*-HOCO. The initial energy distribution typically decays rapidly due to the combined effects of fast chemical reaction and vibrational deactivation of excess population at high energies. Because the time scales of the initial transient (fast) and the thermal reaction (slow) are reasonably well-separated even under the most extreme conditions, as shown in Figure 3, the rate constant can be determined by totally neglecting the subsequent slow regeneration of HO + CO by steady-state

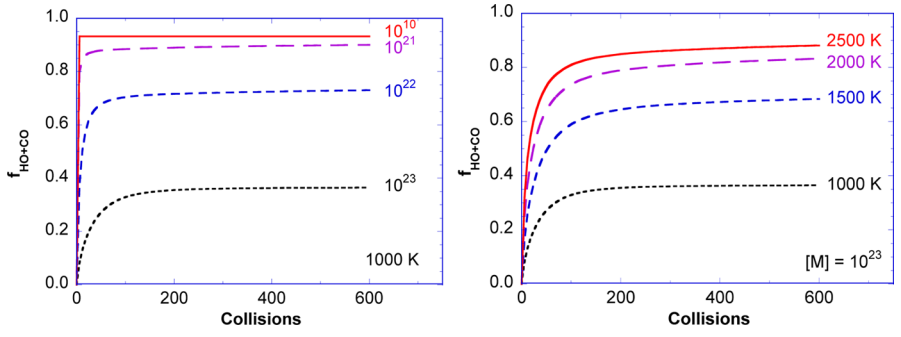

Figure 3. Simulations of chemically activated (excited) HOCO reacting to regenerate HO + CO (left) at 1000 K and various He concentrations, and (right) at [He] = 10^{23} cm^{-3} and various temperatures.

dx.doi.org/10.1021/jp311928w | J. Phys. Chem. A 2013, 117, 821−835

reaction,[112] or by making further corrections when the rate of the slow regeneration is significant.[127,128] The total fraction $f_{HO+CO}(t_{transient})$ of HO regenerated rapidly during the initial fast transient is used in eq 6 to obtain the rate constant for the net forward reaction:

$$k_1 = [1 - f_{HO+CO}(t_{transient})]k_{1a,\infty} \quad (6)$$

In the present calculations at $P = 0$, the steady-state regeneration of HO following the fast initial transient is extremely slow and can be neglected. Generally, the errors are largest when the subsequent steady-state regeneration of HO is fastest. This situation is illustrated in Figure 3, right, where the regeneration of HO at 2500 K and [He] = 10^{23} cm^{-3} is still perceptible to the eye, even after 600 collisions. However, even in this, the most extreme case, f_{HO+CO} increased only from 0.85 to 0.88 in the span from 200 to 400 collisions; this corresponds to a difference of only ~25% in the computed rate constant. Thus, the error introduced by totally neglecting the slow steady-state regeneration of HO is insignificant except at simultaneous high temperature and high pressure, but it is always less than 25%, which is tolerable for present purposes. Thus, in the present work, we neglect the slow steady-state regeneration of HO, but as mentioned above, the error could be further reduced at high pressures and temperatures by taking the subsequent slow process into account.[127,128]

Rate Constants for HO + CO. Rate constants for HO + CO in various bath gases have been measured by many research groups. Most of the measurements were carried out in He, but some groups have also measured rate constants in Ar, N_2, CF_4, and SF_6 bath gases.

For helium bath gas, it is convenient to compare the computed rate constants with experimental rate constants measured near the temperatures used by Fulle et al.,[35] who covered the widest range of temperatures and pressures in their work. In Figures 4–8, the computed rate constants are compared with experimental measurements from the literature. In these semilog plots of rate constant vs $\log_{10}$[He], the rate constant has a sigmoidal shape as it increases from the $P = 0$ intercept, passes through intermediate pressures, and then approaches the high-pressure limit. In each plot, the 1D master equation results are shown as the heavy solid line

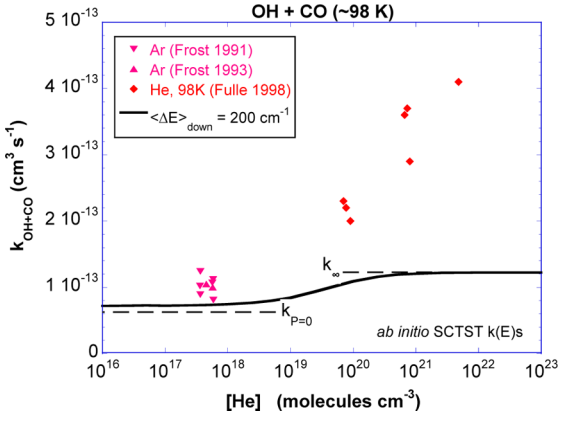

Figure 4. Rate constants for HO + CO in He bath at 98 K. Experimental data are shown as points (errors of ~20%). The heavy solid line is the rate constant predicted by the 1D master equation with α(He) = −200 cm^{-1}. Also shown are the $P = 0$ and $P = \infty$ rate constants predicted by the 2D master equation with ab initio SCTST rate constants.

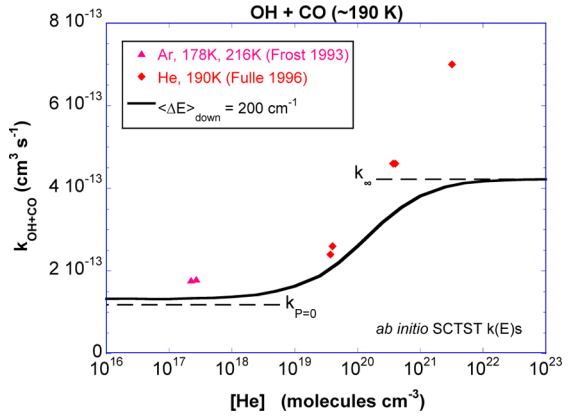

Figure 5. Rate constants for HO + CO in He bath at 190 K. Experimental data are shown as points (errors of ~20%). The heavy solid line is the rate constant predicted by the 1D master equation with α(He) = −200 cm^{-1}. Also shown are the $P = 0$ and $P = \infty$ rate constants predicted by the 2D master equation with ab initio SCTST rate constants.

(corresponding to α(He) = 200 cm^{-1}), and the 2D master equation results for the low- and high-pressure limits are shown as horizontal thin dashed lines. All of the rate constants obtained in the present work are tabulated in the Supporting Information.

At the lowest pressures, the experimental rate constants are in good agreement with the computed $P = 0$ limit, even for $T \leq$ 300 K. Even at ~98 K, the computed rate constants are accurate to within a factor of ×2, and the experimental scatter is at least ±25%. If the factor of ×2 at 98 K is attributed to errors in the calculated energies, it corresponds to $|\Delta E| = 0.14$ kcal mol^{-1}, which is smaller than the energy errors anticipated for the HEAT 345Q protocol.

All of the plots show the small discrepancies between the 1D master equation and 2D master equation results at $P = 0$. As explained in the Appendix, the small discrepancy arises at least in part from how the centrifugal corrections are implemented in the 1D and 2D master equations. Essentially, the 2D master equation takes a ratio of $k(E,J)$ at each J and averages the ratio over the thermal distribution of J; in contrast, the 1D master equation with centrifugal corrections averages each $k(E,J)$ over the thermal distribution before using the ratio of $k(E)$s. Other approximations introduced to simplify the centrifugal corrections may also contribute to the discrepancy. Nevertheless, although noticeable, the discrepancy is small for the HO + CO system.

At very high pressures, the experimental rate constants do not clearly indicate that they have reached a high-pressure limit. At 298 K and very high pressures (Figure 6), the data of Forster et al. and Fulle et al. have a tendency to roll over as if they are approaching the high-pressure limit, but the stated experimental error bars of ~20% are about twice as large as the difference between the experiments and the present calculations, as shown in Figure 6. At temperatures > 300 K (Figures 7 and 8), the experimental He pressures are not high enough to reach the predicted high-pressure limits.

At lower temperatures (Figures 4 and 5), the experimental rate constants also do not show any clear indications of reaching the high-pressure limit, but their magnitudes at high pressures greatly exceed the predicted limits. Unless the weakly bound prereactive complex preceding TS1 exerts some dynamical effect on the total rate of reaction, it is difficult to

dx.doi.org/10.1021/jp311928w | J. Phys. Chem. A 2013, 117, 821–835

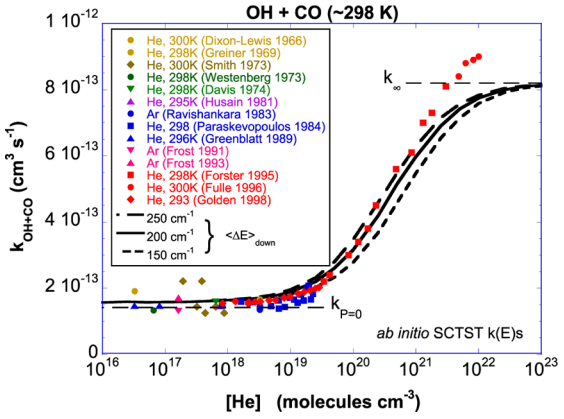

Figure 6. Rate constants for HO + CO in He bath at 298 K. Experimental data (errors of ~20%) are shown as points. The heavy solid line is the rate constant predicted by the 1D master equation with $\alpha(\mathrm{He}) = -200\ \mathrm{cm}^{-1}$ (the upper and lower dashed lines correspond to 250 and 150 cm^{-1}, respectively). Also shown are the $P = 0$ and $P = \infty$ rate constants predicted by the 2D master equation with ab initio SCTST rate constants.

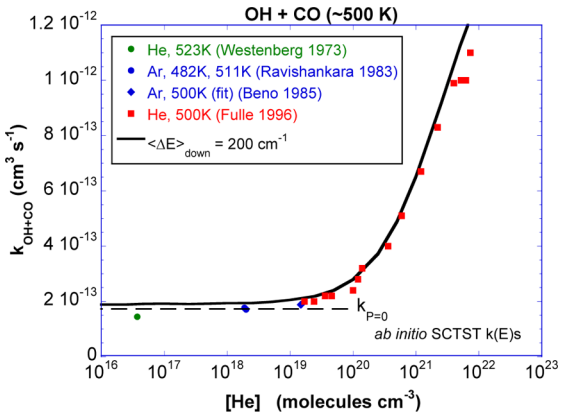

Figure 7. Rate constants for HO + CO in He bath at 500 K. Experimental data are shown as points (errors of ~20%). The heavy solid line is the rate constant predicted by the 1D master equation with $\alpha(\mathrm{He}) = -200\ \mathrm{cm}^{-1}$. Also shown is the $P = 0$ rate constant predicted by the 2D master equation with ab initio SCTST rate constants.

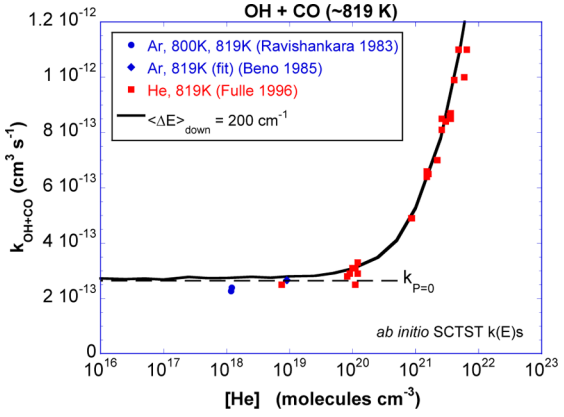

Figure 8. Rate constants for HO + CO in He bath at 819 K. Experimental data are shown as points (errors of ~20%). The heavy solid line is the rate constant predicted by the 1D master equation with $\alpha(\mathrm{He}) = -200\ \mathrm{cm}^{-1}$. Also shown is the $P = 0$ rate constant predicted by the 2D master equation with ab initio SCTST rate constants.

identify possible reasons for this behavior. However, if statistical rate theory (i.e., in a two-transition state model) is applicable to the prereactive complex, its most likely effect will be to reduce the overall reaction rate, not increase it. Furthermore, its geometry (linear OH−CO) does not favor formation of the new C−O bond.

Another possible explanation for this discrepancy at very low temperatures and very high pressures is that complexes or dimers present in the experimental reaction mixtures react significantly with HO radicals. If HO radicals react efficiently by reactions other than reaction 1a, the experimental rate constants for loss of HO will be enhanced. Helium is not expected to form dimers or complexes even at the lowest temperatures and highest pressures achieved in the experiments, but CO and the photolytic precursors used to generate the HO free radical might be present in concentrations high enough to pose a problem. The van der Waals potential well-depths (ε, given in parentheses) of CO (105 K, ref 129), N_2O (249 K, ref 129), O_3 (161 K, ref 130), and CH_4 (153 K, ref 129) are small but are perhaps large enough to account for some formation of complexes at $T < 200$ K. The possible presence of dimers or complexes remains an open question.

The global rate constant for loss of HO radicals increases with pressure until it reaches its high-pressure limit; the rate of increase depends on the magnitude of the energy transfer parameter α. The dependence on $\alpha(\mathrm{He})$ is shown in Figure 6, where the solid line corresponds to $\alpha(\mathrm{He}) = 200\ \mathrm{cm}^{-1}$. As pointed out above, this value produces good agreement with the experimental data for He bath gas at temperatures ≥ 298 K. Slightly better agreement between the 1D master equation calculations and experiments can be obtained by using $\alpha(\mathrm{He}) = 150\ \mathrm{cm}^{-1}$ at 298 K and pressures $\lesssim 1$ bar, as shown in Figure 9.

The linear scales in Figure 9 help to reveal subtle features in the HO + CO data that are not as visible in the semilog plots. First, the agreement between models and most experiments would be improved if the computed rate constant at $P = 0$ was

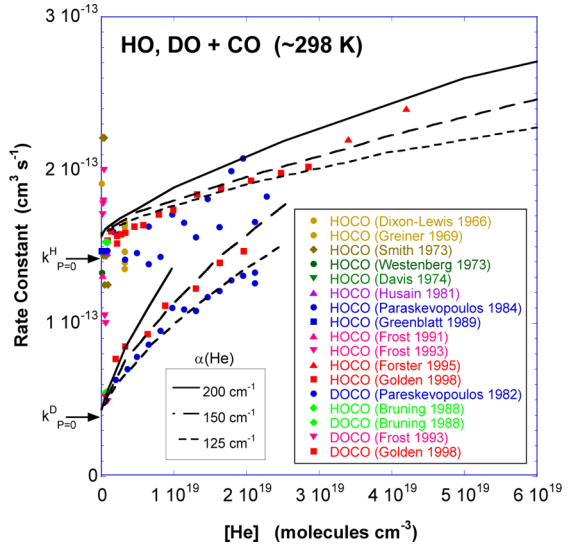

Figure 9. Pressure-dependent rate constants (helium bath gas) for HO + CO and for DO + CO. In each case, the solid and dashed lines correspond to simulations obtained using three values of $\alpha(\mathrm{He})$, as shown. The $P = 0$ intercepts for the HO and DO isotopologues predicted using the 2D master equation with ab initio SCTST rate constants are shown by the arrows on the y axis.

dx.doi.org/10.1021/jp311928w | J. Phys. Chem. A 2013, 117, 821−835

lowered by ∼15% to the value obtained using the exact solution of the 2D master equation. This suggests that the ab initio SCTST rate constants are highly accurate. The experimental data and calculations agree reasonably well for α(He) = 125 or 150 cm^{-1}, but if the ∼15% offset was eliminated, the optimal value of α(He) would be close to 175 cm^{-1}. However, the data show considerable scatter between and even within data sets, except for the set of Golden et al.[36] In particular, the data of Paraskevopolous et al.[20] exhibit considerable scatter. The data of Golden et al. exhibit modest curvature, which is mimicked by the 1D master equation results.

Other bath gases have been investigated at 298 K and pressures of $\lesssim$1 bar, and we have modeled experimental data for Ar, N_2, CF_4, and SF_6 for those conditions. The results are summarized in Table 2. Inspection of Table 2 shows that the values found for α in the present work are reasonably consistent with previous work. In particular, α(Ar) ≈ α(N_2), and both α(CF_4) and α(SF_6) are large, suggesting that collisional energy transfer involving CF_4 and SF_6 is very efficient, as expected because of their low-frequency vibrational modes.[131]

H/D Kinetic Isotope Effect. The rate constant for the reaction DO + CO has been determined in a number of experiments, at pressures up to about one atmosphere and mostly at temperatures around ∼298 K. In some cases, the same group has studied both the HO and the DO reaction, but in separate experiments, not in rate measurements with both species present simultaneously at the same bath gas pressure and temperature.[20,24,31,36,57] For this reason, we have simply plotted the two rate constants separately. This approach also makes the experimental scatter and inconsistencies readily apparent.

The theoretical rate constants are based on harmonic frequencies, vibrational anharmonicities, and reaction enthalpies for the DO + CO PES computed using the same levels of theory and basis sets that were used for the normal isotope. Since the vibrational frequencies and rotational constants for the DOCO isomers differ from those of the HOCO species, it was *not* assumed that the energy transfer parameters are the same. Instead, rate constants for both isotopes were computed for three assumed values of α(He), as noted in Figure 9. Like the HO + CO rate data, the rate constants for DO + CO exhibit modest curvature that is mimicked by the 1D master equation simulations. In all cases, the slopes of the theoretical rate constants with buffer gas concentration are greatest at the lowest pressures. This behavior combined with experimental scatter makes it difficult to identify the actual zero pressure intercept of the experimental data. In addition, there is a small displacement of the data of Golden et al.[36] from those of Paraskevopolous et al.[20] However, most of the data are consistent with α(He) = 125 to 150 cm^{-1} for the DOCO isotopologues.

For the DO + CO isotopologue, there is again a small discrepancy between the P = 0 intercepts predicted by the 2D master equation and the 1D numerical results at 300 K: 3.87 × 10^{-14} vs 4.25 × 10^{-14} cm^3 s^{-1}, respectively, as shown in Figure 9. The H/D KIEs at 300 K predicted using the 2D and the 1D methods are 3.66 and 3.80, respectively. The H/D KIEs at P = 0 and P = ∞ predicted using the 2D master equation, which are expected to be more accurate, are shown as a function of 1/T in Figure 10.

Considering the scatter displayed in Figure 9, the uncertainty in the experimental H/D KIE at P = 0 is significant. The exclusively low pressure data for HO + CO are widely

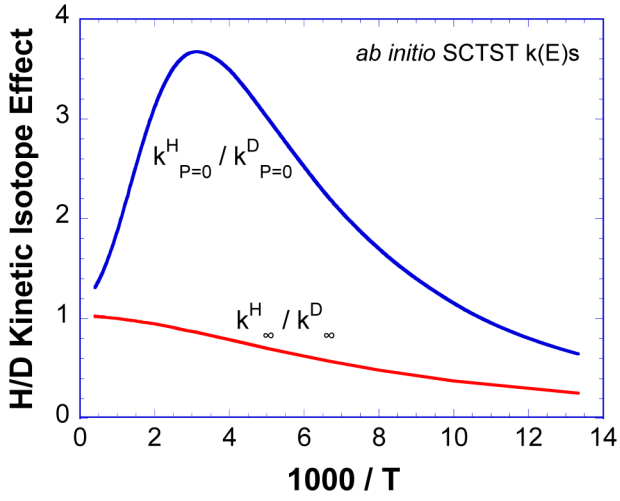

Figure 10. H/D kinetic isotope effects for reaction R1 predicted using the 2D master equation with ab initio SCTST rate constants. The two lines correspond to the limiting values at P = 0 and at P = ∞.

scattered, but clusters of data points are found near both 1.5 × 10^{-13} and 1.3 × 10^{-13} cm^3 s^{-1}. The pressure-dependent data of Golden et al.[36] have relatively high precision and appear to have an intercept near 1.5 × 10^{-13} cm^3 s^{-1}, but if the plot is curved like the theoretical results, the intercept may be somewhat lower. The pressure dependent data of Paraskevopolous et al.[24] are quite scattered and appear to have an intercept of roughly 1.5 × 10^{-13} cm^3 s^{-1}. The data for DO + CO are more limited: a cluster of low pressure data points falls near 5 × 10^{-14} cm^3 s^{-1}, but the pressure-dependent data of Golden et al.[36] and Paraskevopolous et al.[20] require risky extrapolations to P = 0. We estimate that the intercepts are roughly 0.5 × 10^{-13} and 0.43 × 10^{-13} cm^3 s^{-1}, respectively. Taking all of these results into consideration, we think it is likely that the H/D KIE at zero pressure is about 3.2 with an uncertainty of perhaps 10%. This value for the KIE is ∼13% lower than the 3.66 obtained in the present work with the 2D master equation with SCTST rate constants.

Chen and Marcus have argued that the H/D KIE at low pressure can only be explained by abandoning RRKM theory, which does not fit the data.[70,103] Their RRKM model employed frequencies computed using CCSD(T)/6-31G(d,p) and quantum mechanical tunneling based on an Eckart potential energy barrier. As an alternative to RRKM theory, they proposed a heuristic non-RRKM model that could be adjusted to fit the data. The ab initio SCTST rate constants employed in the present work are based on a PES computed with substantially larger basis sets. Unlike standard TST with Eckart tunneling corrections, the SCTST rate constants include full anharmonic vibrational coupling and tunneling along the curved reaction path. The H/D KIE at P = 0 computed in the present work is in much better agreement with the experimental data than were the calculations of Chen and Marcus. This suggests that their difficulty in matching the experimental H/D KIEs was largely due to limitations of the less accurate methods that they had available.

Since the experiments and theory are now in quite reasonable agreement, we conclude that there is no compelling reason to postulate nonstatistical behavior in the HO + CO reaction. However, it is important to bear in mind that nonstatistical effects may still be present since intramolecular vibrational energy redistribution may be incomplete due to the

brief lifetimes of the HOCO isomers.[56,132−134] We expect that future improvements in both experiments and theory will further reduce the small difference that currently exists.

CONCLUSIONS

The ab initio results obtained using the 2D master equation with SCTST microcanonical rate constants are in very good agreement with the experimental data for the HO + CO and the DO + CO reactions at zero pressure. Experimental rate constants approaching the high-pressure limit are not available for comparison at temperatures above 300 K. At lower temperatures, the predicted high-pressure limit rate constants are much smaller than the experimental data. Furthermore, the relative difference increases as the temperature is lowered further, possibly because prereactive complexes and/or dimers may be important in the experiments, but their influence was not recognized; they were not considered in the calculations. This question warrants further investigation, both theoretical and experimental.

Explicit 2D master equation codes are not available for calculations at intermediate pressures, although such codes were demonstrated some time ago.[135−137] Instead, a general purpose 1D master equation code (MultiWell) with ab initio SCTST microcanonical rate constants was employed in the conventional manner. At low and intermediate pressures, the 1D master equation results are in good agreement with the experimental data for He bath gas at all temperatures when the conventional exponential-down model is used with a single empirical parameter for energy transfer: α = 200 cm^{-1}. This parameter roughly corresponds to the average energy transferred in deactivation collisions. Even better agreement with experimental data near 300 K is seen when α is reduced somewhat.

The 1D and 2D master equations have the same high-pressure limits, but a comparison of results at the zero pressure limit shows a discrepancy of ≤15%. A detailed analysis of the discrepancy at P = 0 shows that it arises at least in part from approximations used in making centrifugal corrections. These approximations can be eliminated in future development of an explicit 2D master equation code.

The predicted rate constants for both HO and DO with CO are in reasonable agreement with the experiments, especially when experimental errors and the deficiencies of the theory are taken into account. The discrepancy found earlier by Chen and Marcus has been greatly reduced in the present calculations, which provide a better treatment for both tunneling and vibrational anharmonicity. Considering the uncertainties in the experimental kinetic isotope effect measurements for this reaction, there is no *need* at present to postulate nonstatistical (i.e., non-RRKM) rate constants.

A very important conclusion from the present work is that the combination of high-level quantum chemistry methods (i.e., CCSD(T) theory and the HEAT protocol) with SCTST constitutes a powerful method for predicting both thermal and microcanonical rate constants.

APPENDIX

A. Centrifugal Corrections in MultiWell

This section is included in order to fully document the centrifugal corrections employed in the present work. A detailed discussion can also be found in the current MultiWell User Manual.[114]

The master equation can be written as a function of either of two equivalent sets of independent variables: E,J or ε,J. The total rovibrational energy E can be written in terms of the active energy ε and angular momentum quantum number J: $E = \varepsilon + BJ(J+1)$, where B is the rotational constant of the reactant in a unimolecular reaction.[101,122,138,139] In terms of the active energy, the time-dependent master equation can be written as[128]

$$\frac{\mathrm{d}N(\varepsilon', J', t)}{\mathrm{d}t} = F'(\varepsilon', J', t) + \sum_J \int_0^\infty R(\varepsilon', J'; E, J)N(\varepsilon, J; t)\mathrm{d}\varepsilon - \sum_J \int_0^\infty R(\varepsilon, J; \varepsilon', J')N(\varepsilon', J', t)\mathrm{d}\varepsilon - \sum_{i=1}^{\text{channels}} k_i(\varepsilon', J')N(\varepsilon', J', t) \quad \text{(A1)}$$

where the primed ε' and J' refer to the current state and the unprimed quantities refer to a different state of the excited species that is undergoing reaction. In eq A1, $N(\varepsilon',J',t)\mathrm{d}\varepsilon'$ is the concentration of a chemical species with active energy in the range ε' to $\varepsilon' + \mathrm{d}\varepsilon'$; $R(\varepsilon,J;\varepsilon',J')$ is the (pseudo-first-order) rate coefficient for collisional energy transfer from initial energy E' to energy E and quantum number J' to J; $F'(\varepsilon',J',t)\mathrm{d}\varepsilon'$ is a source term (e.g. thermal-, chemical-, or photoactivation, or isomerization); and $k_i(\varepsilon',J')$ is the unimolecular reaction rate constant for molecules at energy ε' and rotational quantum number J' reacting via the ith reaction channel.

To reduce the 2DME to a 1DME, we first assume that the rotational population distribution describing the adiabatic rotations is always Boltzmann:

$$P_e(J) = Q_J^{-1} g_J \exp(-E_J/k_BT) \quad \text{(A2a)}$$

where $g_J = 2J + 1$ for a 2D symmetric top (which is typically assumed) and other forms for 1D rotors or spherical tops; the rotational energy E_J and the rotational partition function Q_J for the adiabatic rotor(s) are given by:

$$E_J = BJ(J+1) \quad \text{(A2b)}$$

$$Q_J = \sum_J g_J \exp(-E_J/k_BT) \quad \text{(A2c)}$$

The constant B is the rotational constant. By using these expressions, the concentrations can be written as

$$N(\varepsilon, J, t) = N(\varepsilon, t)P_e(J) \quad \text{(A3)}$$

In the same spirit, we assume the source function produces the same rotational distribution:

$$F'(\varepsilon', J', t) = F(\varepsilon', t)P_e(J') \quad \text{(A4)}$$

Although recent trajectory calculations show that the assumption is probably not accurate,[140,141] we follow Smith and Gilbert[100] and Miller et al.[142] in adopting the pragmatic assumption that the collision rates in eq A1 can be written in a separable form:

$$R(\varepsilon, J; \varepsilon', J') = R(\varepsilon, \varepsilon')P_e(J) \quad \text{(A5)}$$

where $R(\varepsilon, \varepsilon')$ has no dependence on angular momentum and can be expressed as the product of the total vibrationally

inelastic collision frequency (ω) multiplied by the collision step-size distribution, $P(\varepsilon, \varepsilon')$, which expresses the probability that a molecule initially in the energy range from ε' to $\varepsilon' + d\varepsilon'$ will undergo an inelastic transition to the energy range ε to $\varepsilon + d\varepsilon$:

$$R(\varepsilon, J; \varepsilon', J') = \omega P(\varepsilon, \varepsilon') P_e(J) \tag{A6}$$

where ω is the collision frequency and $P(\varepsilon, \varepsilon')$ is the normalized collision step-size distribution. Smith and Gilbert showed that the master equation can be solved approximately when using this separable form. In MultiWell, this separable form is adopted pragmatically in order to obtain a semi-analytical solution to the master equation. (Miller and coworkers have further generalized the function postulated by Smith and Gilbert,[100] and the details may be found in their papers.[101,142])

After substituting these expressions in the master equation and noting that the sums over J are equal to unity because $P_e(J)$ is normalized, it is found that every term contains the factor $P_e(J')$. By summing every term in eq A1 over J' and noting that the sum equals unity in each term except the last, we obtain the general form of the 1D master equation implemented in MultiWell:

$$\frac{dN(\varepsilon', t)}{dt} = F(\varepsilon', t) + \omega \int_0^\infty [P(\varepsilon'; \varepsilon) N(\varepsilon, t) - P(\varepsilon; \varepsilon') N(\varepsilon', t)] d\varepsilon - N(\varepsilon', t) \sum_{i=1}^{\text{channels}} \langle k_i(\varepsilon') \rangle_J \tag{A7a}$$

where $\langle k_i(E') \rangle_J$ is the RRKM specific rate constant, averaged over the rotational energy distribution

$$\langle k_i(\varepsilon') \rangle_J = \sum_{J'=0}^{J'_{max}} P_e(J') k_i(\varepsilon', J') \tag{A7b}$$

The upper limit of the summation (J'_{max}) in eq A7b corresponds to the largest angular momentum quantum number for which the potential well defining the unimolecular reactant still exists.

The averaging of $k_i(\varepsilon',J')$ over the rotational energy distribution may be carried out by first writing the expression for the specific rate constant $k(\varepsilon',J')$[115]

$$k(\varepsilon', J') = \frac{L^\ddagger}{h} \frac{G^\ddagger(\varepsilon^+, J')}{\rho(\varepsilon', J')} \tag{A8}$$

where $L^\ddagger$ is the reaction path degeneracy, h is Planck's constant, $G^\ddagger(\varepsilon^+,J')$ is the sum of states of the transition state (or cumulative reaction probability) as a function of the active energy ε^+ in the transition state, and $\rho(\varepsilon',J')$ is the density of vibrational states of the reactant when the rotational quantum number is J'. The various energies are related as follows (see Figure 2.3-1 in the MultiWell User Manual):

$$\varepsilon' + E_J = \varepsilon^+ + E_0 + E_J^+ \tag{A9a}$$

or

$$\varepsilon' = \varepsilon^+ + E_0 + \Delta E_J \tag{A9b}$$

where E_J and E_J^+ are the energies of the adiabatic rotations in the reactant and in the transition state, respectively, and $\Delta E_J = E_J^+ - E_J$, where $E_J^+ = B^+J(J+1)$ and $\Delta E_J = (1 - B/B^+)E_J^+$.

For reactions involving bond fission, the rotational constant B^+ for a rigid rotor transition state is smaller than that for the reactant and $\Delta E_J < 0$. As the angular momentum quantum number J' increases, the quantity $(E_0 - \Delta E_J)$ approaches zero. In other words, the reactant well and the effective critical energy for reaction both vanish when J' is large enough: J'_{max} is the largest value of J' for which the well still exists. For $J' > J'_{max}$, $k(\varepsilon',J')$ is not defined. When $B^+ \leq B$ for rigid rotors, $J'_{max} = \infty$.

When the rate constant is averaged over the equilibrium rotational population distribution, the result is

$$\langle k(\varepsilon', J') \rangle_J = Q_J^{-1} \sum_{J'=0}^{J'_{max}} k(\varepsilon', J') g_J \exp[-(E_J^+ - \Delta E_J)/k_B T] \tag{A10}$$

Care must be taken, however, because the rate constant is only defined at energies $E' \geq (E_0 + \Delta E_J)$. Because for a prolate symmetric top $\Delta E_J \leq 0$, the reaction threshold may be significantly lower in energy than E_0, the critical energy for $J = 0$.

Here, it is pragmatically assumed that the K-rotor is active and the K quantum number has no restrictions other than conservation of energy.[119,121,122,143,144] This has been shown to be an excellent approximation, except when the rotational constant is large and at very low energies.[119,120] As a result, the approximate density of states of the reactant molecule has no explicit dependence on the J quantum number. Another pragmatic approximation was introduced by Marcus, who replaced ΔE_J with $\langle \Delta E_J \rangle = (1 - B/B^+)\langle E_J^+ \rangle$ and obtained an approximate 1D specific rate constant, which does not retain any explicit dependence on the rotational state J':

$$k_a(\varepsilon') = \frac{L^\ddagger}{h} \frac{G^\ddagger(\varepsilon' - E_0 - \langle \Delta E_J \rangle)}{\rho(\varepsilon')} \tag{A11}$$

where the subscript "a" was used by Marcus to denote the approximate form. It is convenient to use the same approximation every time ΔE_J appears, and we obtain

$$\langle k(\varepsilon') \rangle_J = k_a(\varepsilon') \exp(\langle \Delta E_J \rangle / k_B T) Q_J^{-1} \sum_J g_J \exp[-E_J^+/k_B T] \tag{A12}$$

The remaining sum over J' is recognized as Q_J^+, the rotational partition function for the transition state. Marcus found $\langle E_J^+ \rangle = lk_BT/2$ (where l is the number of adiabatic rotors), the average rotational energy in the transition state, by weighting the average according to the reactive flux.[115,121,144,145] Using this value of $\langle \Delta E_J \rangle \approx (1 - B/B^+)lk_BT/2 = (1 - I^+/I)lk_BT/2$, where I and I^+ are the moments of inertia for the adiabatic rotor in the reactant and the transition state, respectively,[115] the final result can be written as

$$\langle k(\varepsilon') \rangle_J = k_a(\varepsilon') \left(\frac{B}{B^+}\right)^{l/2} \exp\left(\frac{l}{2}\left[1 - \frac{B}{B^+}\right]\right) \tag{A13}$$

where the ratio of the (classical) rotational partition functions has been replaced by the ratio of the rotational constants or moments of inertia, and l is the number of adiabatic rotors. Usually it is assumed that $l = 2$.

These simplified forms perform well in master equation simulations, although the energy transfer parameters may differ

dx.doi.org/10.1021/jp311928w | J. Phys. Chem. A 2013, 117, 821−835

to some extent from other treatments. These possible differences are not considered to be very important because no current master equation treatment of energy transfer is known to be correct and because energy transfer parameters and collision step-size distributions generally are not known from other sources, but are simply used as empirical fitting parameters.

B. Accuracy of the 1D Master Equation with Centrifugal Corrections at $P = 0$

It is apparent that a small discrepancy exists between the $P = 0$ intercept computed from eq 1 and that computed by MultiWell at pressures where the pressure is negligible. This discrepancy exists because of the approximate centrifugal corrections employed in the MultiWell master equation code, which were introduced by Marcus in order to reduce the formal 2D master equation (depending on E,J) to a 1D master equation (depending on E).[115] Other approaches exist for reducing the 2D master equation to 1D (in particular, see papers by Gilbert and Smith[99,100] and by Miller and Klippenstein[101]), but all such approaches are ad hoc approximations to the explicit 2D master equation, as discussed elsewhere.[128,140]

In the explicit 2D master equation at $P = 0$ for the HO + CO reaction, a microcanonical equilibrium is first assumed and then averaged over a thermal distribution of E and J, as expressed in eq 1. This equation can also be expressed in terms of the unimolecular rate constants for the reactions of the *cis*- and *trans*-HOCO, regarded here as a single species undergoing internal rotation. It is useful to compare the exact 2D master equation solution to that obtained numerically by the MultiWell master equation code.

To express eq 1 in terms of the HOCO unimolecular reactions, we employ the canonical equilibrium constant for reaction R1, which is given by $K_1(T) = [Q_{HOCO}/(Q_{HO} \times Q_{CO})] \times \exp(-\Delta H_1/k_B T)$, where Q_i is the total partition function for the ith species (i = HOCO, CO, and HO) evaluated from its zero-point energy, and ΔH_1 is the enthalpy of reaction R1 at 0 K. We also note that $K_1(T)$ is equal to k_1/k_{-1}, the ratio of rate constants for the forward and reverse directions. Equation 4 is used to define the microcanonical rate constant, $k_{-1}(E',J)$, for the reverse of reaction R1, which has the same CRP as the forward reaction. Here, E' is the total rovibrational internal energy of HOCO. Equation 4 is also used to obtain the microcanonical rate constants for reactions 2 and 3. With these substitutions, eq 1 takes the following form:

$$k_{P=0}(T) = \frac{K_1(T)}{Q_{HOCO}} \sum_{J=0}^{+\infty} (2J+1) \int_{-\Delta H_1}^{+\infty} \rho_{HOCO}(E',J) \left\{ \frac{k_{-1}(E',J) k_{23}(E',J)}{k_{-1}(E',J) + k_{23}(E',J)} \right\} e^{(-E'/k_B T)} dE' \quad \text{(B1)}$$

where $\rho_{HOCO}(E',J)$ is the density of states of HOCO. In this expression, microcanonical equilibrium is assumed in writing the ratio $R(E',J) = k_{23}(E',J)/[k_{-1}(E',J) + k_{23}(E',J)]$, which is the fraction of energized HOCO leading to H + CO_2. At each J, the integrand in eq B1 is equal to this ratio multiplied by the chemical activation energy distribution.

As described above, the MultiWell master equation code is formulated[138] in terms of the active energy, ε', and therefore, $E' = \varepsilon' + BJ(J+1)$. By substituting this expression for E' and changing the order of summation and integration, eq B1 can be written as

$$k_{P=0}(T) = \frac{K_1(T)}{Q_{HOCO}} \int_{-\Delta H_1}^{+\infty} \sum_{J=0}^{+\infty} (2J+1)\, e^{\left(-\frac{BJ(J+1)}{k_B T}\right)} R(\varepsilon', J)\, \rho_{HOCO}(\varepsilon', J) k_{-1}(\varepsilon', J)\, e^{(-\varepsilon'/k_B T)} d\varepsilon' \quad \text{(B2)}$$

Equation B2 is written in a form to emphasize that it can be regarded as an average over the ε,J chemical activation distribution, which is defined as

$$p_{CA}(\varepsilon, J) = \frac{1}{N_{CA}} (2J+1)\, e^{\left(-\frac{BJ(J+1)}{k_B T}\right)} \rho_{HOCO}(\varepsilon, J) k_{-1}(\varepsilon, J)\, e^{(-\varepsilon/k_B T)} \quad \text{(B3a)}$$

where the normalization constant is

$$N_{CA} = \int_{-\Delta H_1}^{+\infty} \sum_{J=0}^{+\infty} (2J+1)\, e^{\left(-\frac{BJ(J+1)}{k_B T}\right)} \rho_{HOCO}(\varepsilon, J) k_{-1}(\varepsilon, J)\, e^{(-\varepsilon/k_B T)} d\varepsilon \quad \text{(B3b)}$$

The normalization constant can be recognized as the product of the high-pressure limit rate constant for reaction −R1 multiplied by the partition function for HOCO:

$$N_{CA} = k_{-1,\infty}(T) Q_{HOCO} \quad \text{(B4)}$$

With these substitutions, the rate constant for reaction R1 at the $P = 0$ limit can be written as the average:

$$k_{P=0}(T) = K_1(T) k_{-1,\infty}(T) \left\langle \frac{k_{23}(\varepsilon, J)}{k_{-1}(\varepsilon, J) + k_{23}(\varepsilon, J)} \right\rangle_{CA} \quad \text{(B5)}$$

where the subscript "CA" indicates the average over the 2D chemical activation energy distribution.

Equation B5, an alternative to eq 1, is the exact solution of the 2D master equation for rate constant $k_{P=0}(T)$. This expression stands in contrast to the corresponding expression for the 1D master equation employing the centrifugal corrections described above. The centrifugal corrections amount to independently averaging each microcanonical $k_i(\varepsilon,J)$ over the thermal distribution of J. Recall that the MultiWell simulations are initialized with a 1D chemical activation distribution that depends only on ε'. In the absence of collisional energy transfer, the numerical solution of the 1D master equation with centrifugal corrections can be written formally as

$$k_{P=0}(T) = k_{-1,\infty}(T) K_1(T) \left\langle \frac{\langle k_{23}(\varepsilon, J)\rangle_J}{\langle k_{-1}(\varepsilon, J)\rangle_J + \langle k_{23}(\varepsilon, J)\rangle_J} \right\rangle_{CA'} \quad \text{(B6)}$$

where the subscript "CA'" denotes averaging over the 1D chemical activation distribution. Thus, the two approaches are not equivalent because, in eq B5, the ratio is always evaluated with all of the rate constants at the same ε,J, while in eq B6, the rate constants are averaged separately.

We conclude from this analysis that the small discrepancy at $P = 0$ between the MultiWell 1D master equation with centrifugal corrections and the explicit collision-free 2D master equation arises at least in part from the differences between eqs B5 and B6. It is worth noting that careful rotational averaging of the 2D master equation, although considerably more

dx.doi.org/10.1021/jp311928w | J. Phys. Chem. A 2013, 117, 821−835

cumbersome, leads to the exact $P = 0$ limit, as has been pointed out by others.[96−101]

■ ASSOCIATED CONTENT

Supporting Information

Optimized geometries, rovibrational parameters, anharmonic vibrational constants, and energies for various species in the HO + CO and DO + CO reaction are given, as are tabulated rate constants. This material is available free of charge via the Internet at http://pubs.acs.org.

■ AUTHOR INFORMATION

Corresponding Author

*E-mail : jfstanton@mail.utexas.edu (J.F.S.); jrbarker@umich.edu. (J.R.B.).

Notes

The authors declare no competing financial interest.

■ ACKNOWLEDGMENTS

J.R.B. thanks Horst Hippler, David Golden, Michael Frenklach, Stephen Klippenstein, and James Miller for useful discussions. R.E.W. thanks DOE for support. J.R.B. thanks the National Science Foundation (Atmospheric and Geospace Sciences) and NASA (Upper Atmospheric Research Program). J.F.S. and T.L.N. are supported by the Robert A. Welch Foundation (Grant F-1283) and the Department of Energy, Office of Basic Energy Sciences (Contract Number DE-FG02- 07ER15884).

■ REFERENCES

(1) Gardiner, W. C., Jr., Ed. *Combustion Chemistry*; Springer-Verlag: New York, 2012.
(2) Finlayson-Pitts, B. J.; Pitts, J. N., Jr. *Chemistry of the Upper and Lower Atmosphere*; Academic Press: San Diego, CA, 2000.
(3) Yung, Y. L.; DeMore, W. B. *Photochemistry of Planetary Atmospheres*; Oxford University Press: Oxford, U.K., 1999.
(4) Dixon-Lewis, G.; Wilson, W. E.; Westenberg, A. A. *J. Chem. Phys.* **1966**, *44*, 2877−2884.
(5) Greiner, N. R. *J. Chem. Phys.* **1969**, *51*, 5049−5051.
(6) Dean, A. M.; Kistiakowsky, G. B. *J. Chem. Phys.* **1971**, *54*, 1718−1725.
(7) Dryer, F.; Naegeli, D.; Glassman, I. *Combust. Flame* **1971**, *17*, 270−272.
(8) Izod, T. P. J.; Kistiakowsky, G. B.; Matsuda, S. *J. Chem. Phys.* **1971**, *55*, 4425−4432.
(9) Stuhl, F.; Niki, H. *J. Chem. Phys.* **1972**, *57*, 3671−3677.
(10) Westenberg, A. A.; deHaas, N. J. *J. Chem. Phys.* **1973**, *58*, 4061−4065.
(11) Smith, I. W. M.; Zellner, R. *J. Chem. Soc., Faraday Trans. II* **1973**, *69*, 1617−1627.
(12) Howard, C. J.; Evenson, K. M. *J. Chem. Phys.* **1974**, *61*, 1943−1952.
(13) Davis, D. D.; Fischer, S.; Schiff, R. *J. Chem. Phys.* **1974**, *61*, 2213−2219.
(14) Trainor, D. W.; Vonrosenberg, C. W., Jr. *Chem. Phys. Lett.* **1974**, *29*, 35−38.
(15) Gordon, S.; Mulac, W. A. *Int. J. Chem. Kinet.* **1975**, *7*, 289−299.
(16) Perry, R. A.; Atkinson, R.; Pitts, J. N., Jr. *J. Chem. Phys.* **1977**, *67*, 5577−5584.
(17) Overend, R.; Paraskevopoulos, G. *Chem. Phys. Lett.* **1977**, *49*, 109−111.
(18) Biermann, H. W.; Zetzsch, C.; Stuhl, F. *Ber. Bunsenges. Phys. Chem.* **1978**, *82*, 633.
(19) Clyne, M. A. A.; Holt, P. M. *J. Chem. Soc., Faraday Trans. 2* **1979**, *75*, 569−581.
(20) Paraskevopoulos, G.; Irwin, R. S. *Chem. Phys. Lett.* **1982**, *93*, 138−143.
(21) Ravishankara, A. R.; Thompson, R. L. *Chem. Phys. Lett.* **1983**, *99*, 377−381.
(22) Hofzumahaus, A.; Stuhl, F. *Ber. Bunsenges. Phys. Chem.* **1984**, *88*, 557−561.
(23) Niki, H.; Maker, P. D.; Savage, C. M.; Breitenbach, L. P. *J. Phys. Chem.* **1984**, *88*, 2116−2119.
(24) Paraskevopoulos, G.; Irwin, R. S. *J. Chem. Phys.* **1984**, *80*, 259−266.
(25) Jonah, C. D.; Mulac, W. A.; Zeglinski, P. *J. Phys. Chem.* **1984**, *88*, 4100−4104.
(26) DeMore, W. B. *Int. J. Chem. Kinet.* **1984**, *16*, 1187−1200.
(27) Beno, M. F.; Jonah, C. D.; Mulac, W. A. *Int. J. Chem. Kinet.* **1985**, *17*, 1091−1101.
(28) Smith, I. W. M.; Williams, M. D. *Ber. Bunsenges Phys. Chem.* **1985**, *89*, 319−320.
(29) Hynes, A. J.; Wine, P. H.; Ravishankara, A. R. *J. Geophys. Res., [Atmos.]* **1986**, *91*, 1815−1820.
(30) Frost, M. J.; Salh, J. S.; Smith, I. W. M. *J. Chem. Soc., Faraday Trans.* **1991**, *87*, 1037−1038.
(31) Frost, M. J.; Sharkey, P.; Smith, I. W. M. *J. Phys. Chem.* **1993**, *97*, 12254−12259.
(32) Smith, I. W. M. *Mon. Not. R. Astron. Soc.* **1988**, *234*, 1059−1063.
(33) Forster, R.; Frost, M.; Fulle, D.; Hamann, H. F.; Hippler, H.; Schlepegrell, A.; Troe, J. *J. Chem. Phys.* **1995**, *103*, 2949−2958.
(34) Lissianski, V.; Yang, H.; Qin, Z.; Mueller, M. R.; Shin, K. S.; Gardiner, W. C., Jr. *Chem. Phys. Lett.* **1995**, *240*, 57−62.
(35) Fulle, D.; Hamann, H. F.; Hippler, H.; Troe, J. *J. Chem. Phys.* **1996**, *105*, 983−1000.
(36) Golden, D. M.; Smith, G. P.; McEwen, A. B.; Yu, C. L.; Eiteneer, B.; Frenklach, M.; Vaghjiani, G. L.; Ravishankara, A. R.; Tully, F. P. *J. Phys. Chem. A* **1998**, *102*, 8598−8606.
(37) Hottel, H. C.; Williams, G. C.; Nerheim, N. M.; Schneider, G. R. OH + CO. In *10th (International) Symposium on Combustion*; The Combustion Institute: Pittsburgh, PA, 1964; p 129.
(38) Westenberg, A. A.; Fristrom, R. M. OH + CO. In *10th (International) Symposium on Combustion*; The Combustion Institute: Pittsburgh, PA, 1964; p 473.
(39) Dixon-Lewis, G.; Sutton, M. M.; Williams, A. OH + CO. In *10th (International) Symposium on Combustion*; The Combustion Institute: Pittsburgh, PA, 1964; p 495.
(40) Heath, G. A.; Pearson, G. S. OH + CO. In *11th (International) Symposium on Combustion*; The Combustion Institute: Pittsburgh, PA, 1966; p 967.
(41) Wilson, W. E., Jr.; O'Donovan, J. T.; Fristrom, R. M. OH + CO. In *12th (International) Symposium on Combustion*; The Combustion Institute: Pittsburgh, PA, 1968; p 907.
(42) Baldwin, R. R.; Walker, R. W.; Webster, S. J. *Combust. Flame* **1970**, *15*, 167−172.
(43) Atri, G. M.; Baldwin, R. R.; Jackson, D.; Walker, R. W. *Combust. Flame* **1977**, *30*, 1−12.
(44) Peeters, J.; Mahnen, G. OH + CO. In *14th (International) Symposium on Combustion*; The Combustion Institute: Pittsburgh, PA, 1972; p 133.
(45) Eberus, K. H.; Hoyermann, K.; Wagner, H. G. OH + CO. In *14th (International) Symposium on Combustion*; The Combustion Institute: Pittsburgh, PA, 1972; p 147.
(46) Vandooren, J.; Peeters, J.; Tiggelen, P. J. V. OH + CO. In *15th (International) Symposium on Combustion*; The Combustion Institute: Pittsburgh, PA, 1974; p 745.
(47) Wooldridge, M. S.; Hanson, R. K.; Bowman, C. T. OH + CO. In *25th (International) Symposium on Combustion*; The Combustion Institute: Pittsburgh, PA, 1994; p 741.
(48) Brabbs, R. A.; Belles, F. E.; Brokaw, R. S. OH + CO. In *13th (International) Symposium on Combustion*; The Combustion Institute: Pittsburgh, PA, 1970; p 129.
(49) Gardiner, W. C., Jr.; Mallard, W. G.; McFarland, M.; Morinaga, K.; Owen, J. H.; Rawlins, W. T.; Takeyama, T.; Walker, B. F. OH + CO. In *14th (International) Symposium on Combustion*; The Combustion Institute: Pittsburgh, PA, 1972; p 61.

(50) Biordi, J. C.; Lazzara, C.; Papp, J. F. OH + CO. In *15th (International) Symposium on Combustion*; The Combustion Institute: Pittsburgh, PA, 1974; p 917.
(51) Smith, I. W. M. *Chem. Phys. Lett.* **1977**, *49*, 112−115.
(52) Stevens, C. M.; Kaplan, L.; Gorse, R.; Durkee, S.; Compton, M.; Cohen, S.; Bielling, K. *Int. J. Chem. Kinet.* **1980**, *12*, 935−948.
(53) Röckmann, T.; Brenninkmeijer, C. A. M.; Saueressig, G.; Bergamaschi, P.; Crowley, J. N.; Fischer, H.; Crutzen, P. J. *Science* **1998**, *281*, 544−546.
(54) Feilberg, K. L.; Sellevåg, S. R.; Nielsen, C. J.; Griffith, D. W. T.; Johnson, M. S. *Phys. Chem. Chem. Phys.* **2002**, *4*, 4687−4693.
(55) Feilberg, K. L.; Johnson, M. S.; Nielsen, C. J. *Phys. Chem. Chem. Phys.* **2005**, *7*, 2318−2323.
(56) Alagia, M.; Balucani, N.; Casavecchia, P.; Stranges, D.; Volpi, G. G. *J. Chem. Phys.* **1993**, *98*, 8341−8344.
(57) Brunning, J.; Derbyshire, D. W.; Smith, I. W. M.; Williams, M. D. *J. Chem. Soc., Faraday Trans. 2* **1988**, *84*, 105−119.
(58) Clements, T. G.; Continetti, R. E.; Francisco, J. S. *J. Chem. Phys.* **2002**, *117*, 6478−6488.
(59) Johnson, C. J.; Continetti, R. E. *J. Phys. Chem. Lett.* **2010**, *1*, 1895−1899.
(60) Johnson, C. J.; Poad, B. L. J.; Shen, B. B.; Continetti, R. E. *J. Chem. Phys.* **2011**, *134*, 171106.
(61) Ma, J. Y.; Guo, H. *Chem. Phys. Lett.* **2011**, *511*, 193−195.
(62) McLean, A. D.; Ellinger, Y. *Chem. Phys.* **1985**, *94*, 25−41.
(63) Kudla, K.; Koures, A. G.; Harding, L. B.; Schatz, G. C. *J. Chem. Phys.* **1992**, *96*, 7465−7473.
(64) Francisco, J. S. *J. Chem. Phys.* **1997**, *107*, 9039−9045.
(65) Li, Y.; Francisco, J. S. *J. Chem. Phys.* **2000**, *113*, 7963−7970.
(66) Duncan, T. V.; Miller, C. E. *J. Chem. Phys.* **2000**, *113*, 5138−5140.
(67) Yu, H.-G.; Muckerman, J. T.; Sears, T. J. *Chem. Phys. Lett.* **2001**, *349*, 547−554.
(68) Aoyagi, M.; Kato, S. *J. Chem. Phys.* **1988**, *88*, 6409−6418.
(69) Zhu, R. S.; Diau, E. G. W.; Lin, M. C.; Mebel, A. M. *J. Phys. Chem. A* **2001**, *105*, 11249−11259.
(70) Chen, W.-C.; Marcus, R. A. *J. Chem. Phys.* **2005**, *123*, 094307.
(71) Song, X.; Li, J.; Hou, H.; Wang, B. *J. Chem. Phys.* **2006**, *125*, 094301.
(72) Nguyen, T. L.; Xue, B.; Weston, R. E., Jr.; Barker, J. R.; Stanton, J. F. *J. Phys. Chem. Lett.* **2012**, *3*, 1549−1553.
(73) Senosiain, J. P.; Musgrave, C. B.; Golden, D. M. *Int. J. Chem. Kinet.* **2003**, *35*, 464−474.
(74) Senosiain, J. P.; Klippenstein, S. J.; Miller, J. A. *Proc. Combust. Inst.* **2005**, *30*, 945−953.
(75) Larson, C. W.; Stewart, P. H.; Golden, D. M. *Int. J. Chem. Kinet.* **1988**, *20*, 27−40.
(76) Lamb, J. J.; Mozurkewich, M.; Benson, S. W. *J. Phys. Chem.* **1984**, *88*, 6435−6441.
(77) Valero, R.; Kroes, G.-J. *J. Chem. Phys.* **2002**, *117*, 8736.
(78) Joshi, A. V.; Wang, H. *Int. J. Chem. Kinet.* **2006**, *38*, 57−73.
(79) Schatz, G. C.; Dyck, J. *Chem. Phys. Lett.* **1992**, *188*, 11−15.
(80) Clary, D. C.; Schatz, G. C. *J. Chem. Phys.* **1993**, *99*, 4578−4589.
(81) Feilberg, K. L.; Billing, G. D.; Johnson, M. S. *J. Phys. Chem. A* **2001**, *105*, 11171−11176.
(82) Guo, H. *Int. Rev. Phys. Chem.* **2012**, *31*, 1−68.
(83) Ma, J.; Li, J.; Guo, H. *J. Phys. Chem. Lett.* **2012**, *3*, 2482−2486.
(84) Xie, C. J.; Li, J.; Xie, D. Q.; Guo, H. *J. Chem. Phys.* **2012**, 137.
(85) Li, J.; Wang, Y.; Jiang, B.; Ma, J.; Dawes, R.; Xie, D.; Bowman, J. M.; Guo, H. *J. Chem. Phys.* **2012**, *136*, 041103.
(86) Garcia, E.; Saracibar, A.; Zuazo, L.; Laganà, A. *Chem. Phys.* **2007**, *332*, 162−175.
(87) Lakin, M. J.; Troya, D.; Schatz, G. C.; Harding, L. B. *J. Chem. Phys.* **2003**, *119*, 5848−5859.
(88) Kudla, K.; Schatz, G. C.; Wagner, A. F. *J. Chem. Phys.* **1991**, *95*, 1635−1647.
(89) Miller, W. H. *Faraday Discuss. Chem. Soc.* **1977**, *62*, 40−46.
(90) Miller, W. H.; Hernandez, R.; Handy, N. C.; Jayatilaka, D.; Willets, A. *Chem. Phys. Lett.* **1990**, *172*, 62−68.
(91) Cohen, M. J.; Handy, N. C.; Hernandez, R.; Miller, W. H. *Chem. Phys. Lett.* **1992**, *192*, 407−416.
(92) Hernandez, R.; Miller, W. H. *Chem. Phys. Lett.* **1993**, *214*, 129−136.
(93) Nguyen, T. L.; Stanton, J. F.; Barker, J. R. *Chem. Phys. Lett.* **2010**, *499*, 9−15.
(94) Nguyen, T. L.; Stanton, J. F.; Barker, J. R. *J. Phys. Chem. A* **2011**, *115*, 5118−5126.
(95) Stanton, J. F.; Gauss, J.; Harding, M. E.; Szalay, P. G.; Auer, A. A.; Bartlett, R. J.; Benedikt, U.; Berger, C.; Bernholdt, D. E.; Bomble, Y. J.; et al. *CFOUR*, a quantum chemical program package; University of Texas: Autsin, TX, 2009.
(96) Troe, J. *J. Chem. Phys.* **1977**, *66*, 4745−4757.
(97) Just, T.; Troe, J. *J. Phys. Chem.* **1980**, *84*, 3068−3072.
(98) Troe, J. *J. Chem. Soc., Faraday Trans.* **1994**, *90*, 2303−2317.
(99) Smith, S. C.; Gilbert, R. G. *Int. J. Chem. Kinet.* **1988**, *20*, 979−990.
(100) Smith, S. C.; Gilbert, R. G. *Int. J. Chem. Kinet.* **1988**, *20*, 307−329.
(101) Miller, J. A.; Klippenstein, S. J. *J. Phys. Chem. A* **2006**, *110*, 10528−10544.
(102) Barker, J. R.; Nguyen, T. L.; Stanton, J. F. *J. Phys. Chem. A* **2012**, *116*, 6408−6419.
(103) Chen, W. C.; Marcus, R. A. *J. Chem. Phys.* **2006**, *124*, 024306.
(104) Marcus, R. A. *J. Phys. Chem. C* **2009**, *113*, 14598−14608.
(105) Tajti, A.; Szalay, P. G.; Csaszar, A. G.; Kallay, M.; Gauss, J.; Valeev, E. F.; Flowers, B. A.; Vazquez, J.; Stanton, J. F. *J. Chem. Phys.* **2004**, *121*, 11599−11613.
(106) Bomble, Y. J.; Vazquez, J.; Kallay, M.; Michauk, C.; Szalay, P. G.; Csaszar, A. G.; Gauss, J.; Stanton, J. F. *J. Chem. Phys.* **2006**, *125*, 064108.
(107) Harding, M. E.; Vazquez, J.; Ruscic, B.; Wilson, A. K.; Gauss, J.; Stanton, J. F. *J. Chem. Phys.* **2008**, *128*, 114111.
(108) Almlof, J.; Taylor, P. R. *J. Chem. Phys.* **1987**, *86*, 4070−4077.
(109) Mills, I. M. Vibration-Rotation Structure in Asymmetric- and Symmetric-Top Molecules. In *Molecular Spectroscopy: Modern Research*; Rao, K. N., Mathews, C. W., Eds.; Academic Press: New York, 1972; Vol. *1*, pp 115−140.
(110) Feller, D.; Dixon, D. A.; Francisco, J. S. *J. Phys. Chem. A* **2003**, *107*, 1604−1617.
(111) Miller, W. H. *Acc. Chem. Res.* **1976**, *9*, 306−312.
(112) Barker, J. R. *Int. J. Chem. Kinet.* **2001**, *33*, 232−245.
(113) Barker, J. R. *Int. J. Chem. Kinet.* **2009**, *41*, 748−763.
(114) Barker, J. R.; Ortiz, N. F.; Preses, J. M.; Lohr, L. L.; Maranzana, A.; Stimac, P. J.; Nguyen, T. L.; Kumar, T. J. D. *MultiWell-2012.2 Software*; University of Michigan: Ann Arbor, MI, 2012. http://aoss.engin.umich.edu/multiwell/.
(115) Marcus, R. A. *J. Chem. Phys.* **1965**, *43*, 2658−2661.
(116) Nguyen, T. L.; Barker, J. R. *J. Phys. Chem. A* **2010**, *114*, 3718−3730.
(117) Basire, M.; Parneix, P.; Calvo, F. *J. Chem. Phys.* **2008**, *129*, 081101.
(118) Wang, F.; Landau, D. P. *Phys. Rev. Lett.* **2001**, *86*, 2050−2053.
(119) Current, J. H.; Rabinovitch, B. S. *J. Chem. Phys.* **1963**, *38*, 783−795.
(120) Aubanel, E. E.; Wardlaw, D. M.; Zhu, L.; Hase, W. L. *Int. Rev. Phys. Chem.* **1991**, *10*, 249−286.
(121) Holbrook, K. A.; Pilling, M. J.; Robertson, S. H. *Unimolecular Reactions*, 2nd ed.; Wiley: Chichester, U.K., 1996.
(122) Forst, W. *Unimolecular Reactions. A Concise Introduction*; Cambridge University Press: Cambridge, U.K., 2003.
(123) Barker, J. R. *Chem. Phys.* **1983**, *77*, 301−318.
(124) Gillespie, D. T. *J. Comput. Phys.* **1976**, *22*, 403−434.
(125) Gillespie, D. T. *J. Phys. Chem.* **1977**, *81*, 2340−2361.
(126) Francisco, J. S.; Muckerman, J. T.; Yu, H.-G. *Acc. Chem. Res.* **2010**, *43*, 1519−1526.
(127) Golden, D. M. *Z. Phys. Chem.* **2011**, *225*, 969−982.
(128) Golden, D. M.; Barker, J. R. *Combust. Flame* **2011**, *158*, 602−617.

(129) Hippler, H.; Troe, J.; Wendelken, H. J. *J. Chem. Phys.* **1983**, *78*, 6709.
(130) Troe, J. *J. Chem. Phys.* **1977**, *66*, 4758−4775.
(131) Barker, J. R.; Yoder, L. M.; King, K. D. *J. Phys. Chem. A* **2001**, *105*, 796−809.
(132) Scherer, N. F.; Sipes, C.; Bernstein, R. B.; Zewail, A. H. *J. Chem. Phys.* **1990**, *92*, 5239−5259.
(133) Ionov, S. I.; Brucker, G. A.; Jaques, C.; Valachovic, L.; Wittig, C. *J. Chem. Phys.* **1993**, *99*, 6553−6561.
(134) Brouard, M.; Hughes, D. W.; Kalogerakis, K. S.; Simons, J. P. *J. Chem. Phys.* **2000**, *112*, 4557−4571.
(135) Jeffrey, S. J.; Gates, K. E.; Smith, S. C. *J. Phys. Chem.* **1996**, *100*, 7090−7096.
(136) Venkatesh, P. K.; Dean, A. M.; Cohen, M. H.; Carr, R. W. *J. Chem. Phys.* **1997**, *107*, 8904−8916.
(137) Venkatesh, P. K.; Dean, A. M.; Cohen, M. H.; Carr, R. W. *J. Chem. Phys.* **1999**, *111*, 8313−8329.
(138) Gilbert, R. G.; Smith, S. C. *Theory of Unimolecular and Recombination Reactions*; Blackwell Scientific: Oxford, U.K., 1990.
(139) Pilling, M. J.; Robertson, S. H. *Annu. Rev. Phys. Chem.* **2003**, *54*, 245−275.
(140) Barker, J. R.; Weston, R. E., Jr. *J. Phys. Chem. A* **2010**, *114*, 10619−10633.
(141) Barker, J. R.; Weston, R. E., Jr. *J. Phys. Chem. A* **2012**, *116*, 799−799.
(142) Miller, J. A.; Klippenstein, S. J.; Raffy, C. *J. Phys. Chem. A* **2002**, *106*, 4904−4913.
(143) Forst, W. *Theory of Unimolecular Reactions*; Academic Press: New York, 1973.
(144) Robinson, P. J.; Holbrook, K. A. *Unimolecular Reactions*; Wiley-Interscience: London, U.K., 1972.
(145) Marcus, R. A. *J. Chem. Phys.* **1970**, *52*, 1018.
(146) Chan, S. C.; Rabinovitch, B. S.; Bryant, J. T.; Spicer, L. D.; Fujimoto, T.; Lin, Y. N.; Pavlou, S. P. *J. Phys. Chem.* **1970**, *74*, 3160−3176.
(147) Hirschfelder, J. O.; Curtiss, C. F.; Bird, R. B. *Molecular Theory of Gases and Liquids*; Wiley: New York, 1964.
(148) Troe, J. *J. Phys. Chem.* **1979**, *83*, 114−126.
(149) Hippler, H.; Troe, J.; Wendelken, H. J. *J. Chem. Phys.* **1983**, *78*, 6709−6717.